



Thermoelastic wave propagation in functionally graded nanohollow cylinders based on nonlocal theory

Xianhui Wang¹ · Yingying Hou¹ · Xiaoming Zhang¹ · Jianguo Yu¹

Received: 15 December 2022 / Accepted: 23 May 2023 / Published online: 19 June 2023
© The Author(s), under exclusive licence to The Brazilian Society of Mechanical Sciences and Engineering 2023

Abstract

In this paper, a mathematical model is established for the thermoelastic circumferential Lamb waves in functionally graded material nonlocal nanohollow cylinders on account of the nonlocal theory and is solved by the proposed stress-based Legendre polynomials approach (SLPA). The SLPA uses stress as unknown quantities. Thus, the nonlocal stress-free boundary conditions can be satisfied directly. It translates the original differential equations to the linear eigenvalue problems, which reduces the solving difficulty. Comparisons with the available results indicate the validity of the presented SLPA. The nonlocal effects on dispersion and attenuation are discussed. The results show that the nonlocal effect is notable on both phase velocity and attenuation of Lamb-like waves, but is feeble on both phase velocity and attenuation of thermal waves. Meanwhile, the nonlocal effect enhances the attenuation of Lamb-like wave before its maximal value, but then suppresses it. The study on escape frequency reveals that it is independent of the geometric radius, boundary conditions, temperature and is just inverse proportion to the nonlocal parameter.

Keywords Thermoelastic waves · Nonlocal theory · Nanocylindrical plates · Legendre polynomials · Escape frequency

1 Introduction

When the characteristic size of microstructure decreases to a certain range, its mechanical properties change significantly, which are called scale effect [1]. Due to the scale effect, the nanostructures possess some peculiar mechanical properties and have great potential for the fabrication of nanomechanical systems. In addition, the nanostructures in engineering often bear the dynamic load represented by elastic waves, which lead to the change of temperature and the corresponding thermoelastic coupling. The thermoelastic coupling is essential in the field of nanomechanical systems [2, 3]. Therefore, the investigation of thermoelastic wave propagation in nanostructures has great significance for the design and development of various nanodevices.

In the current stage, many researchers have concerned on the elastic wave propagation in nanoplates and nanohollow cylinders, which are widely used in

the nanomechanical systems. He et al. [4] investigated the wave propagation in functionally graded materials (FGMs) cylindrical nanoshell by the wave-based method. Arash et al. [5] considered the waves in nonlocal graphene sheets by using the finite element method. Sidhardh and Ray [6] studied the dispersive behavior of the Rayleigh–Lamb waves in a microplate. Wu et al. [7] investigated the Lamb waves in a nanoplate in view of the surface effects. Ebrahimi and Seyfi [8] studied the wave propagation in multi-scale hybrid nanocomposite plates under the aggregation of the nanoparticles. Li and Han [9] analyzed the elastic waves in the nanocomposite annular plates. Aydogdu [10] studied the longitudinal waves in multiwalled carbon nanotubes. Li and Chou [11] discussed the velocities of waves in single-walled carbon nanotubes. Zhang and Yin [12] analyzed the dispersion curves of the guided circumferential waves in double-walled carbon nanotubes.

On the other hand, the investigation of the thermoelastic wave propagation in nanoplates and cylindrical plates is still limited. Othman and Mondal [13] studied the effect of memory-dependent derivative and thermal

✉ Xiaoming Zhang
zxmworld11@163.com

¹ School of Mechanical and Power Engineering, Henan Polytechnic University, Jiaozuo 454003, China

loading on the wave in generalized micropolar thermoelasticity. Ebrahimi et al. [14] proposed an analytical approach to solve the waves in graphene oxide powder reinforced nanoplates with thermal loading. Hosseini and Zhang [15] carried out transient thermoelastic wave response in the FGM graphene platelets-reinforced nanocomposite cylinders by using the modified micromechanical model. Dai et al. [16] analyzed the flexural wave in thermoelastic functionally graded hollow cylindrical structure conveying nanoflow. Selim [17] discussed the thermoelastic longitudinal waves in a single-walled carbon nanotube. Although the thermoelastic waves in nanoplates and the thermoelastic longitudinal waves in hollow cylindrical structures were investigated, the thermoelastic circumferential Lamb waves in nanocylindrical structures were not considered as far as we know.

All above researches are performed based on the non-classical continuum theories [18–22]. Among these non-classical continuum theories, the nonlocal theory [23] is simple and effective in simulating the scale effect of nanostructures. Its theoretical hypothesis has been verified by phonon dispersion experiment and atomic lattice dynamics simulation [24]. In the context of the nonlocal theory, several traditional methods have been extended to study wave propagation in nanostructures, such as finite element method (FEM) [25], global matrix method (GMM) [26, 27], thin-layer method [28] and many other methods [29–34]. However, these methods all need to solve the nonlinear characteristic equation or solve the large-scale equations. When the wave propagation in dissipative nanostructures, for instance, thermoelastic or viscoelastic structures, in which the complex eigenvalues need to be searched in the complex plane, these methods must consume a lot of CPU time. Especially, the GMM is currently only applicable to flat nanoplates. The reason is that the general solutions of nanocylinder plates with nonlocal effect have not yet been obtained.

In summary, there exist two significant limitations on the available investigations of thermoelastic waves in nanoplates: (1) there is a lack of the small-scale and efficient calculation method; (2) the thermoelastic circumferential Lamb waves in nanocylindrical plates were rarely mentioned, although its study is meaningful for quality inspection and material property measurement of nanocylindrical plates. Motivated by these reasons, a mathematical model is established for the thermoelastic circumferential Lamb waves in FGM nonlocal nanohollow cylinders on account of the nonlocal theory and is solved by the proposed stress-based Legendre polynomials approach (SLPA). The conventional Legendre polynomials approach (LPA) has been widely used to solve many kinds

of guided wave propagation problems, such as elasticity [35], viscoelasticity [36], piezoelectric elasticity [37], thermoelasticity [38], reflection and transmission [39] and microstructure with modified couple-stress theory [40]. The existing LPA uses displacement as unknown quantities and satisfies stress-free boundary condition by the rectangular window function. Then the stress is substituted by the displacement through introducing the constitutive relation into the governing equation. However, the existing LPA could not analyze the Lamb wave propagation in nanostructures with nonlocal effect due to the existence of second derivative of stress.

In this article, the proposed SLPA uses stress as unknown quantities. Thus, the nonlocal stress-free boundary conditions can be satisfied directly. Then the displacement is substituted by the stress through introducing the governing equation into the constitutive relation. Finally, the SLPA translates the original wave problems to the linear eigenvalue problems, which brings about much smaller computational difficulty. Comparison with the available results indicates the validity of the presented SLPA. The study on escape frequency implies that it is independent of the geometric radius and is inverse proportion to the nonlocal parameter. Furthermore, the nonlocal effects on dispersion and attenuation are discussed, and some meaningful results are discovered.

2 Mathematical model and solving process

2.1 Mathematical model

The FGM nanocylindrical plates composed of orthotropic materials are studied in this paper, as shown in Fig. 1. Its inner

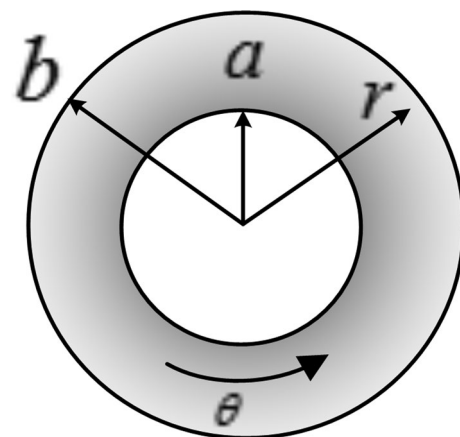


Fig. 1 The section of an FGM nanocylindrical plate

and outer radii are a and b , respectively. The radius thickness ratio $\zeta = b/(b - a)$. Guided waves propagate in the θ -direction. The governing equations of motion and the heat conduction equation can be written in the following forms [41]:

$$\begin{cases} \frac{\partial \sigma_{rr}}{\partial r} + \frac{1}{r} \frac{\partial \sigma_{r\theta}}{\partial \theta} + \frac{\sigma_{rr} - \sigma_{\theta\theta}}{r} = \rho \frac{\partial^2 u_r}{\partial t^2} \\ \frac{\partial \sigma_{r\theta}}{\partial r} + \frac{1}{r} \frac{\partial \sigma_{\theta\theta}}{\partial \theta} + \frac{2\sigma_{r\theta}}{r} = \rho \frac{\partial^2 u_\theta}{\partial t^2} \end{cases} \quad (1a)$$

$$\begin{aligned} K_3 \frac{\partial^2 T}{\partial r^2} + K_1 \left(\frac{1}{r^2} \frac{\partial^2 T}{\partial \theta^2} + \frac{1}{r} \frac{\partial T}{\partial r} \right) - \rho C_e \left(1 + t_0 \frac{\partial}{\partial t} \right) \frac{\partial T}{\partial t} \\ = T_0 \beta_1 \left(1 + t_0 \frac{\partial}{\partial t} \right) \frac{\partial \varepsilon_{\theta\theta}}{\partial t} + T_0 \beta_3 \left(1 + t_0 \frac{\partial}{\partial t} \right) \frac{\partial \varepsilon_{rr}}{\partial t} \end{aligned} \quad (1b)$$

where [42]

$$(1 - \lambda^2 \nabla^2) \sigma_{\theta\theta} = C_{11} \varepsilon_{\theta\theta} + C_{13} \varepsilon_{rr} - \beta_1 T \quad (2a)$$

$$(1 - \lambda^2 \nabla^2) \sigma_{rr} = C_{13} \varepsilon_{\theta\theta} + C_{33} \varepsilon_{rr} - \beta_3 T \quad (2b)$$

$$(1 - \lambda^2 \nabla^2) \sigma_{r\theta} = 2C_{55} \varepsilon_{r\theta} \quad (2c)$$

$$\varepsilon_{\theta\theta} = \frac{1}{r} \frac{\partial u_\theta}{\partial \theta} + \frac{u_r}{r}, \quad \varepsilon_{r\theta} = \frac{1}{2} \left(\frac{1}{r} \frac{\partial u_r}{\partial \theta} + \frac{\partial u_\theta}{\partial r} - \frac{u_\theta}{r} \right), \quad \varepsilon_{rr} = \frac{\partial u_r}{\partial r} \quad (3)$$

Here, σ_{ij} , ε_{ij} and u_i denote the stresses, strains and displacements, respectively; C_{ij} , K_i , β_i , C_e and ρ are the elastic coefficients, material constant characteristics, volume expanding coefficients, specific heat at constant strain and material density, respectively; $T_0 = 296K$; T is the relative temperature, which represents the change relative to T_0 . t and t_0 indicate the time and the relaxation time, respectively. $\nabla^2 = \frac{1}{r} \frac{\partial}{\partial r} \left(r \frac{\partial}{\partial r} \right) + \frac{1}{r^2} \frac{\partial^2}{\partial \theta^2}$ is the Laplacian in coordinate system (r, θ) . λ is the nonlocal parameter [43], which represents the scale effect of nanostructures.

Considering the stress-free boundary condition, the r -direction stress components at the boundary should be zero. Meanwhile, the temperature variation T under isothermal boundary conditions shall also be 0 at the boundary. That is,

$$\left\{ \sigma_{rr}, \sigma_{r\theta}, T \right\} \Big|_{r=a,b} = 0 \quad (4)$$

2.2 Solving process

For the handy analysis, the following nondimensional variables and notations are defined

$$\begin{aligned} \tau_0 = \frac{v_r^2}{k_r} t_0, \quad K = \frac{K_3}{K_1}, \quad \eta = \frac{(\bar{\beta}_1)^2 T_0}{\rho^2 \bar{C}_e v_r^2}, \quad \hat{T} = \frac{T}{T_0}, \\ \hat{r} = \frac{v_r}{k_r} r, \quad \hat{\sigma}_{ij} = \frac{1}{\beta_1 T_0} \sigma_{ij}, \quad \hat{t} = \frac{v_r^2}{k_r} t, \quad \hat{\lambda} = \frac{v_r}{k_r} \lambda \end{aligned} \quad (5)$$

where $v_r = \sqrt{C_{11}/\rho}$ means the velocity of compressional waves. $k_r = \bar{K}_1/\bar{\rho}\bar{C}_e$ indicates the thermal diffusivity in the r direction. η expresses the thermoelastic coupling constant. $\bar{K}_1, \bar{\beta}_1, \bar{\rho}, \bar{C}_e, \bar{C}_{11}$ are $K_1, \beta_1, \rho, C_e, C_{11}$ of the corresponding designated material properties, respectively.

Substituting Eqs.(3,5) in Eqs.(2a), and overwriting $\hat{\sigma}$ as \bullet , it is easy to have

$$(1 - \lambda^2 \nabla^2) \sigma_{\theta\theta} = \frac{C_{11}}{C_{11}} \left(\frac{1}{r} \frac{\partial u_\theta}{\partial \theta} + \frac{u_r}{r} \right) + \frac{C_{13}}{C_{11}} \frac{\partial u_r}{\partial r} - \frac{\beta_1}{C_{11}} T \quad (6)$$

Further applying operator $\frac{\rho}{\rho} \frac{\partial^2}{\partial t^2}$ to both sides of first formula in Eq. (2), it yields

$$\begin{aligned} \frac{\rho}{\rho} (1 - \lambda^2 \nabla^2) \frac{\partial^2 \sigma_{\theta\theta}}{\partial t^2} = \frac{\rho}{\rho} \frac{C_{11}}{C_{11}} \frac{\partial^2}{\partial t^2} \left(\frac{1}{r} \frac{\partial u_\theta}{\partial \theta} + \frac{u_r}{r} \right) \\ + \frac{\rho}{\rho} \frac{C_{13}}{C_{11}} \frac{\partial^2}{\partial t^2} \frac{\partial u_r}{\partial r} - \frac{\rho}{\rho} \frac{\beta_1}{\beta_1} \frac{\partial^2}{\partial t^2} T \end{aligned} \quad (7)$$

Noticing that partial differentiation is

$$\frac{\partial}{\partial r} \left(\rho \frac{\partial^2 \bullet}{\partial t^2} \right) = \frac{\partial \rho}{\partial r} \frac{\partial^2 \bullet}{\partial t^2} + \rho \frac{\partial}{\partial r} \frac{\partial^2 \bullet}{\partial t^2} \quad (8)$$

Equation (7) can be transformed to

$$\begin{aligned} \frac{\rho}{\rho} (1 - \lambda^2 \nabla^2) \frac{\partial^2 \sigma_{\theta\theta}}{\partial t^2} = \frac{\rho}{\rho} \frac{C_{11}}{C_{11}} \frac{\partial^2}{\partial t^2} \left(\frac{1}{r} \frac{\partial u_\theta}{\partial \theta} + \frac{u_r}{r} \right) \\ + \frac{C_{13}}{C_{11}} \frac{\partial^2}{\partial t^2} \left[\frac{\partial}{\partial r} \left(\frac{\rho}{\rho} u_r \right) - u_r \frac{\partial}{\partial r} \left(\frac{\rho}{\rho} \right) \right] - \frac{\rho}{\rho} \frac{\beta_1}{\beta_1} \frac{\partial^2}{\partial t^2} T \end{aligned} \quad (9)$$

Multiplying both sides of Eq. (9) by $\frac{\rho}{\rho}$ and combining with Eqs. (1, 5), we have

$$\begin{aligned}
 & \left(\frac{\rho}{\bar{\rho}}\right)^2 (1 - \lambda^2 \nabla^2) \frac{\partial^2}{\partial t^2} \sigma_{\theta\theta} \\
 &= \frac{\rho}{\bar{\rho}} \frac{C_{11}}{C_{11}} \frac{1}{r} \frac{\partial}{\partial \theta} \left(\frac{\partial \sigma_{r\theta}}{\partial r} + \frac{1}{r} \frac{\partial \sigma_{\theta\theta}}{\partial \theta} + \frac{2\sigma_{r\theta}}{r} \right) \\
 &+ \frac{\rho}{\bar{\rho}} \frac{C_{11}}{C_{11}} \frac{1}{r} \left(\frac{\partial \sigma_{rr}}{\partial r} + \frac{1}{r} \frac{\partial \sigma_{r\theta}}{\partial \theta} + \frac{\sigma_{rr} - \sigma_{\theta\theta}}{r} \right) \\
 &+ \frac{\rho}{\bar{\rho}} \frac{C_{13}}{C_{11}} \frac{\partial}{\partial r} \left(\frac{\partial \sigma_{rr}}{\partial r} + \frac{1}{r} \frac{\partial \sigma_{r\theta}}{\partial \theta} + \frac{\sigma_{rr} - \sigma_{\theta\theta}}{r} \right) \\
 &- \frac{C_{13}}{C_{11}} \frac{\partial}{\partial r} \left(\frac{\rho}{\bar{\rho}} \right) \left(\frac{\partial \sigma_{rr}}{\partial r} + \frac{1}{r} \frac{\partial \sigma_{r\theta}}{\partial \theta} + \frac{\sigma_{rr} - \sigma_{\theta\theta}}{r} \right) \\
 &- \frac{\rho}{\bar{\rho}} \frac{\beta_1}{\beta_1} \frac{\rho}{\bar{\rho}} \frac{\partial^2 T}{\partial t^2}
 \end{aligned} \tag{10a}$$

Similarly, for Eq. (1b) and Eqs. (2b, 2c), it is

$$\begin{aligned}
 \left(\frac{\rho}{\bar{\rho}}\right)^2 (1 - \lambda^2 \nabla^2) \frac{\partial^2}{\partial t^2} \sigma_{r\theta} &= \frac{\rho}{\bar{\rho}} \frac{C_{55}}{C_{11}} \frac{1}{r} \frac{\partial}{\partial \theta} \left(\frac{\partial \sigma_{rr}}{\partial r} + \frac{1}{r} \frac{\partial \sigma_{r\theta}}{\partial \theta} + \frac{\sigma_{rr} - \sigma_{\theta\theta}}{r} \right) \\
 &+ \frac{\rho}{\bar{\rho}} \frac{C_{55}}{C_{11}} \frac{\partial}{\partial r} \left(\frac{\partial \sigma_{r\theta}}{\partial r} + \frac{1}{r} \frac{\partial \sigma_{\theta\theta}}{\partial \theta} + \frac{2\sigma_{r\theta}}{r} \right) \\
 &- \frac{C_{55}}{C_{11}} \frac{\partial}{\partial r} \left(\frac{\rho}{\bar{\rho}} \right) \left(\frac{\partial \sigma_{r\theta}}{\partial r} + \frac{1}{r} \frac{\partial \sigma_{\theta\theta}}{\partial \theta} + \frac{2\sigma_{r\theta}}{r} \right) \\
 &- \frac{\rho}{\bar{\rho}} \frac{C_{55}}{C_{11}} \frac{1}{r} \left(\frac{\partial \sigma_{r\theta}}{\partial r} + \frac{1}{r} \frac{\partial \sigma_{\theta\theta}}{\partial \theta} + \frac{2\sigma_{r\theta}}{r} \right)
 \end{aligned} \tag{10b}$$

$$\begin{aligned}
 & \left(\frac{\rho}{\bar{\rho}}\right)^2 (1 - \lambda^2 \nabla^2) \frac{\partial^2}{\partial t^2} \sigma_{rr} \\
 &= \frac{C_{13}}{C_{11}} \frac{\rho}{\bar{\rho}} \frac{1}{r} \frac{\partial}{\partial \theta} \left(\frac{\partial \sigma_{r\theta}}{\partial r} + \frac{1}{r} \frac{\partial \sigma_{\theta\theta}}{\partial \theta} + \frac{2\sigma_{r\theta}}{r} \right) \\
 &+ \frac{\rho}{\bar{\rho}} \frac{C_{13}}{C_{11}} \frac{1}{r} \left(\frac{\partial \sigma_{rr}}{\partial r} + \frac{1}{r} \frac{\partial \sigma_{r\theta}}{\partial \theta} + \frac{\sigma_{rr} - \sigma_{\theta\theta}}{r} \right) \\
 &+ \frac{\rho}{\bar{\rho}} \frac{C_{33}}{C_{11}} \frac{\partial}{\partial r} \left(\frac{\partial \sigma_{rr}}{\partial r} + \frac{1}{r} \frac{\partial \sigma_{r\theta}}{\partial \theta} + \frac{\sigma_{rr} - \sigma_{\theta\theta}}{r} \right) \\
 &- \frac{C_{33}}{C_{11}} \frac{\partial}{\partial r} \left(\frac{\rho}{\bar{\rho}} \right) \left(\frac{\partial \sigma_{rr}}{\partial r} + \frac{1}{r} \frac{\partial \sigma_{r\theta}}{\partial \theta} + \frac{\sigma_{rr} - \sigma_{\theta\theta}}{r} \right) \\
 &- \frac{\rho}{\bar{\rho}} \frac{\beta_3}{\beta_1} \frac{\rho}{\bar{\rho}} \frac{\partial^2 T}{\partial t^2}
 \end{aligned} \tag{10c}$$

$$\begin{aligned}
 & \frac{K_3}{K_1} \left(\frac{\rho}{\bar{\rho}}\right)^2 \frac{\partial}{\partial t} \frac{\partial^2 T}{\partial r^2} + \frac{K_1}{K_1} \left(\frac{\rho}{\bar{\rho}}\right)^2 \left(\frac{1}{r^2} \frac{\partial}{\partial t} \frac{\partial^2 T}{\partial \theta^2} + \frac{1}{r} \frac{\partial}{\partial t} \frac{\partial T}{\partial r} \right) \\
 &- \frac{C_e}{C_e} \left(\frac{\rho}{\bar{\rho}}\right)^3 \left(1 + \tau_0 \frac{\partial}{\partial t} \right) \frac{\partial^2 T}{\partial t^2} \\
 &= \eta \frac{\rho}{\bar{\rho}} \frac{\beta_1}{\beta_1} \left(1 + \tau_0 \frac{\partial}{\partial t} \right) \left(\frac{1}{r} \frac{\partial}{\partial \theta} \left(\frac{\partial \sigma_{r\theta}}{\partial r} + \frac{1}{r} \frac{\partial \sigma_{\theta\theta}}{\partial \theta} + \frac{2\sigma_{r\theta}}{r} \right) \right. \\
 &\quad \left. + \frac{1}{r} \left(\frac{\partial \sigma_{rr}}{\partial r} + \frac{1}{r} \frac{\partial \sigma_{r\theta}}{\partial \theta} + \frac{\sigma_{rr} - \sigma_{\theta\theta}}{r} \right) \right) \\
 &+ \eta \frac{\beta_3}{\beta_1} \left(1 + \tau_0 \frac{\partial}{\partial t} \right) \left(\frac{\rho}{\bar{\rho}} \frac{\partial}{\partial r} \left(\frac{\partial \sigma_{rr}}{\partial r} + \frac{1}{r} \frac{\partial \sigma_{r\theta}}{\partial \theta} + \frac{\sigma_{rr} - \sigma_{\theta\theta}}{r} \right) \right. \\
 &\quad \left. - \frac{\partial}{\partial r} \left(\frac{\rho}{\bar{\rho}} \right) \left(\frac{\partial \sigma_{rr}}{\partial r} + \frac{1}{r} \frac{\partial \sigma_{r\theta}}{\partial \theta} + \frac{\sigma_{rr} - \sigma_{\theta\theta}}{r} \right) \right)
 \end{aligned} \tag{10d}$$

As the wave propagates in the θ direction, the stress and temperature variables can be expressed as:

$$\begin{cases} \sigma_{\theta\theta}(r, \theta, z, t) = \exp(ikb\theta - i\omega t)U(r) \\ \sigma_{r\theta}(r, \theta, z, t) = \exp(ikb\theta - i\omega t)V(r) \\ \sigma_{rr}(r, \theta, z, t) = \exp(ikb\theta - i\omega t)W(r) \\ T(r, \theta, z, t) = \exp(ikb\theta - i\omega t)X(r) \end{cases} \tag{11}$$

k and ω are the magnitude of the wave vector in the propagation direction and angular frequency, respectively.

Similar to Ref.[36], the material properties could be the following forms

$$\begin{aligned}
 \frac{C_{ij}}{C_{11}}(r) &= C_{ij}^{(m)} \left(\frac{2r - (b+a)}{(b-a)} \right)^m \\
 \frac{\beta_i}{\beta_1}(r) &= \beta_i^{(m)} \left(\frac{2r - (b+a)}{(b-a)} \right)^m \\
 \frac{K_i}{K_1}(r) &= K_i^{(m)} \left(\frac{2r - (b+a)}{(b-a)} \right)^m \\
 \frac{\rho}{\bar{\rho}}(r) &= \rho^{(m)} \left(\frac{2r - (b+a)}{(b-a)} \right)^m, \\
 \frac{C_e}{C_e}(r) &= C_e^{(m)} \left(\frac{2r - (b+a)}{(b-a)} \right)^m \\
 m &= 0, 1, \dots, M
 \end{aligned} \tag{12}$$

Introducing Eqs. (11–12) to Eq. (10), it leads to

$$\left(\frac{2r-b-a}{b-a}\right)^{j+p} \left[\omega^2 \rho^{(j)} \rho^{(p)} \left(1 - \lambda^2 \left(\frac{1}{r} \frac{\partial}{\partial r} + \frac{\partial^2}{\partial r^2} - k^2 b^2 \frac{1}{r^2}\right)\right) U + ikb \rho^{(j)} C_{11}^{(p)} \frac{1}{r} \left(\frac{\partial V}{\partial r} + ikb \frac{1}{r} U + \frac{2V}{r}\right) \right. \\ \left. + \rho^{(j)} C_{11}^{(p)} \frac{1}{r} \left(\frac{\partial W}{\partial r} + ikb \frac{1}{r} V + \frac{W-U}{r}\right) + \rho^{(j)} C_{13}^{(p)} \frac{\partial}{\partial r} \left(\frac{\partial W}{\partial r} + ikb \frac{1}{r} V + \frac{W-U}{r}\right) \right] \\ - \frac{2j}{b-a} \rho^{(j)} C_{13}^{(p)} \left(\frac{2r-b-a}{b-a}\right)^{j+p-1} \left(\frac{\partial W}{\partial r} + ikb \frac{1}{r} V + \frac{W-U}{r}\right) + \omega^2 \rho^{(j)} \rho^{(p)} \beta_1^{(l)} \left(\frac{2r-b-a}{b-a}\right)^{j+p+l} X = 0 \tag{13a}$$

$$\rho^{(j)} \left(\frac{2r-b-a}{b-a}\right)^{j+p} \left[\omega^2 \rho^{(p)} \left(1 - \lambda^2 \left(\frac{1}{r} \frac{\partial}{\partial r} + \frac{\partial^2}{\partial r^2} - k^2 b^2 \frac{1}{r^2}\right)\right) V + ikb C_{55}^{(p)} \frac{1}{r} \left(\frac{\partial W}{\partial r} + ikb \frac{1}{r} V + \frac{W-U}{r}\right) \right. \\ \left. + C_{55}^{(p)} \frac{\partial}{\partial r} \left(\frac{\partial V}{\partial r} + ikb \frac{1}{r} U + \frac{2V}{r}\right) - C_{55}^{(p)} \frac{1}{r} \left(\frac{\partial V}{\partial r} + ikb \frac{1}{r} U + \frac{2V}{r}\right) \right] \\ - \frac{2j}{b-a} \rho^{(j)} C_{55}^{(p)} \left(\frac{2r-b-a}{b-a}\right)^{j+p-1} \left(\frac{\partial V}{\partial r} + ikb \frac{1}{r} U + \frac{2V}{r}\right) = 0 \tag{13b}$$

$$\left(\frac{2r-b-a}{b-a}\right)^{j+p} \left[\omega^2 \rho^{(j)} \rho^{(p)} \left(1 - \lambda^2 \left(\frac{1}{r} \frac{\partial}{\partial r} + \frac{\partial^2}{\partial r^2} - k^2 b^2 \frac{1}{r^2}\right)\right) W + ikb \rho^{(j)} C_{13}^{(p)} \frac{1}{r} \left(\frac{\partial V}{\partial r} + ikb \frac{1}{r} U + \frac{2V}{r}\right) \right. \\ \left. + \rho^{(j)} C_{13}^{(p)} \frac{1}{r} \left(\frac{\partial W}{\partial r} + ikb \frac{1}{r} V + \frac{W-U}{r}\right) + \rho^{(j)} C_{33}^{(p)} \frac{\partial}{\partial r} \left(\frac{\partial W}{\partial r} + ikb \frac{1}{r} V + \frac{W-U}{r}\right) \right] \\ - \frac{2j}{b-a} \rho^{(j)} C_{33}^{(p)} \left(\frac{2r-b-a}{b-a}\right)^{j+p-1} \left(\frac{\partial W}{\partial r} + ikb \frac{1}{r} V + \frac{W-U}{r}\right) + \omega^2 \rho^{(j)} \rho^{(p)} \beta_3^{(l)} \left(\frac{2r-b-a}{b-a}\right)^{j+p+l} X = 0 \tag{13c}$$

$$i\omega \rho^{(j)} \rho^{(p)} K_3^{(l)} \left(\frac{2r-b-a}{b-a}\right)^{j+p+l} \frac{\partial^2 X}{\partial r^2} \\ + i\omega \rho^{(j)} \rho^{(p)} K_1^{(l)} \left(\frac{2r-b-a}{b-a}\right)^{j+p+l} \\ \left(-k^2 b^2 \frac{1}{r^2} X + \frac{1}{r} \frac{\partial X}{\partial r}\right) - \omega^2 \rho^{(j)} \rho^{(p)} \rho^{(m)} C_e^{(l)} \\ \left(\frac{2r-b-a}{b-a}\right)^{j+p+m+l} (1 - i\omega \tau_0) X + \eta \rho^{(j)} \beta_1^{(p)} \\ \left(\frac{2r-b-a}{b-a}\right)^{j+p} (1 - i\omega \tau_0) \\ \left(ikb \frac{1}{r} \left(\frac{\partial V}{\partial r} + ikb \frac{1}{r} U + \frac{2V}{r}\right) \right. \\ \left. + \frac{1}{r} \left(\frac{\partial W}{\partial r} + ikb \frac{1}{r} V + \frac{W-U}{r}\right)\right) \\ + \eta \rho^{(j)} \beta_3^{(p)} \left(\frac{2r-b-a}{b-a}\right)^{j+p} \\ (1 - i\omega \tau_0) \frac{\partial}{\partial r} \left(\frac{\partial W}{\partial r} + ikb \frac{1}{r} V + \frac{W-U}{r}\right) \\ - \frac{2j}{b-a} \eta \rho^{(j)} \beta_3^{(p)} \left(\frac{2r-b-a}{b-a}\right)^{j+p-1} \\ (1 - i\omega \tau_0) \left(\frac{\partial W}{\partial r} + ikb \frac{1}{r} V + \frac{W-U}{r}\right) = 0 \tag{13d}$$

The symbols \bullet' and \bullet'' denote the first and second derivatives.

To resolve Eq. (13), we expand $U(r)$, $V(r)$, $W(r)$ and $X(r)$ to Legendre polynomial series for the traction-free and isothermal boundary conditions according to Eq. (4),

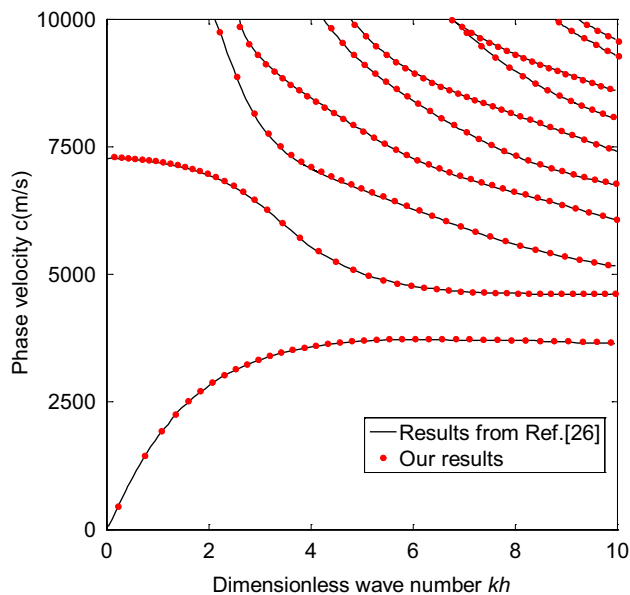


Fig. 2 Comparison with available data [29] for a linear FGM structures

Table 1 Wavenumber k with different N , $\Omega=2$, $\lambda=0.03$, $M=1$

N	1st mode	2nd mode	3rd mode	Thermal mode
2	$5.94 + i*5.39E-5$	$3.10 + i*1.62E-4$	$2.36 + i*5.60E-4$	$0.15 + i*2.53$
4	$5.86 + i*4.40E-5$	$3.32 + i*3.03E-4$	$2.57 + i*4.83E-4$	$0.15 + i*2.54$
6	$5.87 + i*4.67E-5$	$3.33 + i*3.17E-4$	$2.58 + i*4.74E-4$	$0.15 + i*2.54$
8	$5.87 + i*4.78E-5$	$3.33 + i*3.16E-4$	$2.57 + i*4.80E-4$	$0.15 + i*2.54$
10	$5.87 + i*4.84E-5$	$3.33 + i*3.13E-4$	$2.57 + i*4.80E-4$	$0.15 + i*2.54$
12	$5.87 + i*4.84E-5$	$3.33 + i*3.13E-4$	$2.57 + i*4.80E-4$	$0.15 + i*2.54$
14	$5.87 + i*4.84E-5$	$3.33 + i*3.13E-4$	$2.57 + i*4.80E-4$	$0.15 + i*2.54$

Table 2 The properties of the two materials [45, 46]

	C_{11}	C_{13}	C_{33}	C_{55}	ρ	C_e	β_1	β_3	K_1	K_3
Si_3N_4	574	127	433	108	3.2	670	3.22	2.71	55.4	43.5
Al	106.2	52.3	106.2	26.95	2.7	897	4.98	4.98	203.5	203.5

Units: $C_{ij}(10^9 N \cdot m^{-2})$, $C_e(J \cdot kg \cdot deg \cdot m^{-1})$, $\rho(10^3 kg \cdot m^{-3})$, $\beta_i(10^6 N \cdot deg^{-1} \cdot m^{-2})$, $K_i(W/m \cdot K)$

$$\begin{aligned}
 U(r) &= \sum_{n=0}^{\infty} p_n^{(1)} Q_n(r), & V(r) &= (r-a)(r-b) \sum_{n=0}^{\infty} p_n^{(2)} Q_n(r) \\
 W(r) &= (r-a)(r-b) \sum_{n=0}^{\infty} p_n^{(3)} Q_n(r), & X(r) &= (r-a)(r-b) \sum_{n=0}^{\infty} p_n^{(4)} Q_n(r)
 \end{aligned}
 \tag{14}$$

here

$$Q_n(r) = \sqrt{\frac{2m+1}{b-a}} P_n\left(\frac{2r-(b+a)}{b-a}\right) \tag{15}$$

P_n is the n th Legendre polynomial and $p_n^{(i)}$ are the corresponding expansion coefficients.

In fact, with the increase in expansion order n , the influence of higher order on the overall calculation becomes weaker and weaker. Thus, the summation over Eq. (14) could be ended at some value N . Substituting Eq. (14) in Eq. (13) and implementing the orthogonal projection on a linear space composed of a series of Legendre polynomials, we have

$$k^2 \mathbf{A} \mathbf{p} + k \mathbf{B} \mathbf{p} + \mathbf{C} \mathbf{p} = 0 \tag{16}$$

where

$$\begin{aligned}
 \mathbf{A} &= \begin{bmatrix} \mathbf{A}_{11} & 0 & 0 & 0 \\ 0 & \mathbf{A}_{22} & 0 & 0 \\ \mathbf{A}_{31} & 0 & \mathbf{A}_{33} & 0 \\ \mathbf{A}_{41} & 0 & 0 & \mathbf{A}_{44} \end{bmatrix}, & \mathbf{B} &= \begin{bmatrix} 0 & \mathbf{B}_{12} & 0 & 0 \\ \mathbf{B}_{21} & 0 & \mathbf{B}_{23} & 0 \\ 0 & \mathbf{B}_{32} & 0 & 0 \\ 0 & \mathbf{B}_{42} & 0 & 0 \end{bmatrix}, \\
 \mathbf{C} &= \begin{bmatrix} \mathbf{C}_{11} & 0 & \mathbf{C}_{13} & \mathbf{C}_{14} \\ 0 & \mathbf{C}_{22} & 0 & 0 \\ \mathbf{C}_{31} & 0 & \mathbf{C}_{33} & \mathbf{C}_{34} \\ \mathbf{C}_{41} & 0 & \mathbf{C}_{43} & \mathbf{C}_{44} \end{bmatrix}, & \mathbf{p} &= [\mathbf{p}_m^{(1)}, \mathbf{p}_m^{(2)}, \mathbf{p}_m^{(3)}, \mathbf{p}_m^{(4)}]^T.
 \end{aligned}$$

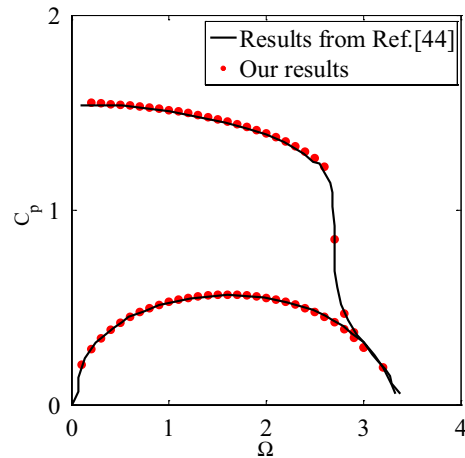


Fig. 3 Comparison with available ones [44] for a nonlocal nanostructures, $\lambda=0.1/0.34$

The detailed expressions of Eq. (16) are shown in Appendix. A new vector \mathbf{q} is introduced,

$$\mathbf{q} = k \mathbf{p} \tag{17}$$

Coupling Eqs. (16) and (17) can obtain,

$$\begin{bmatrix} \mathbf{0} & \mathbf{I} \\ -\mathbf{C} & -\mathbf{B} \end{bmatrix} \begin{bmatrix} \mathbf{p} \\ \mathbf{q} \end{bmatrix} = k \begin{bmatrix} \mathbf{I} & \mathbf{0} \\ \mathbf{0} & \mathbf{A} \end{bmatrix} \begin{bmatrix} \mathbf{p} \\ \mathbf{q} \end{bmatrix} \tag{18}$$

\mathbf{I} is Identity matrix. Thus, the origin nonlinear eigenvalue problems are transformed to the linear eigenvalue problems.

Fig. 4 Phase velocity of the Lamb-like waves with different λ . **a** 1st mode and **b** 2nd mode

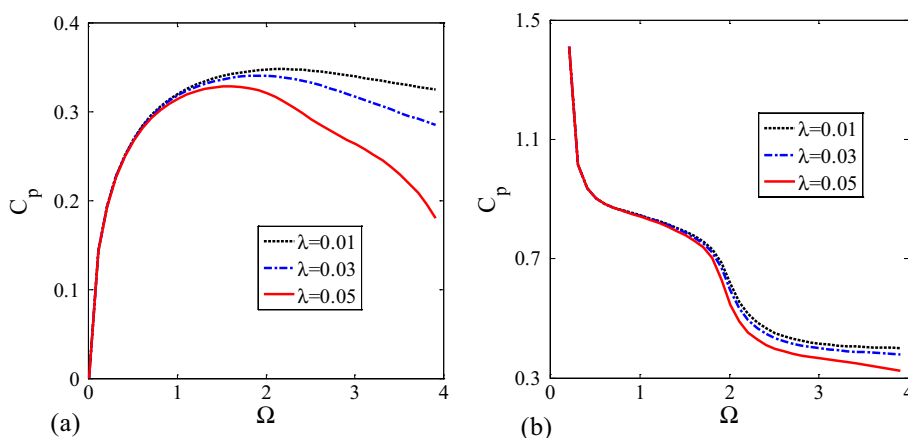


Fig. 5 Attenuation coefficient of the Lamb-like waves with different λ . **a** 1st mode and **b** 2nd mode

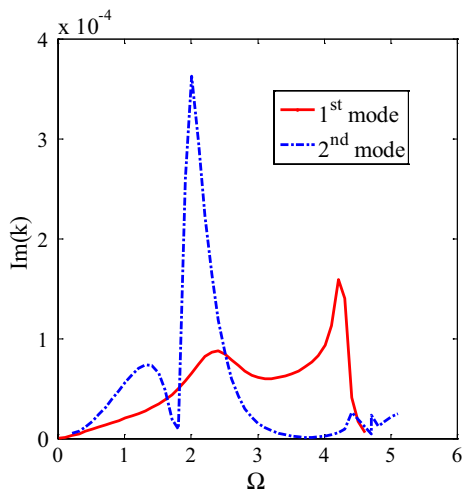
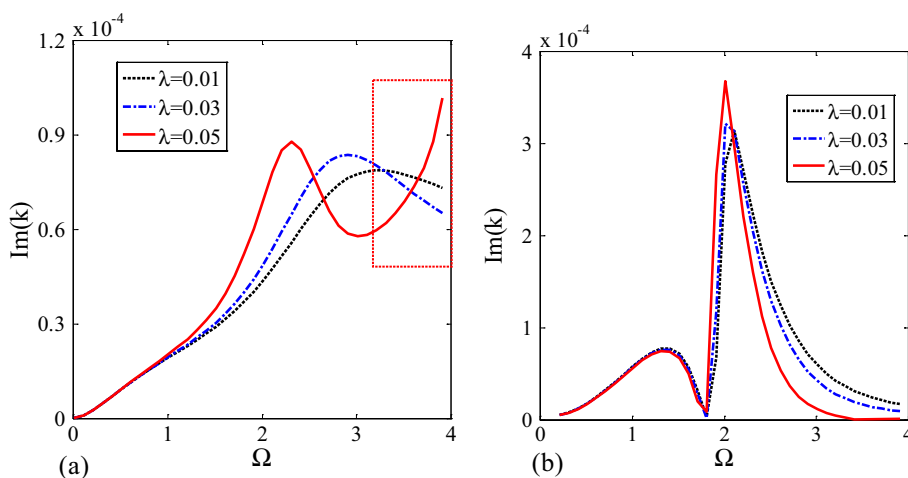


Fig. 6 Attenuation curves of the Lamb-like waves with $\lambda=0.05$

3 Numerical examples

Based on the above formulations, the program for the SLPA is written. The properties of FGM can be expressed as:

$$P(r) = \frac{P_1(r)}{2} \left[1 - \left(\frac{r-a}{b-a} \right)^M \right] + \frac{P_2(r)}{2} \left(\frac{r-a}{b-a} \right)^M \quad (19)$$

where $P_i(r)$ denotes the corresponding property of the i th material. Ω is used to express frequency thickness product. Without explanation, $a=4$ and $b=5$.

3.1 Validity of the SLPA

Due to the lack of available data, the SLPA is validated by wave solutions in the FGM and nonlocal uniform

Fig. 7 Phase velocity and attenuation of the thermal wave with different λ . **a** Phase velocity and **b** attenuation

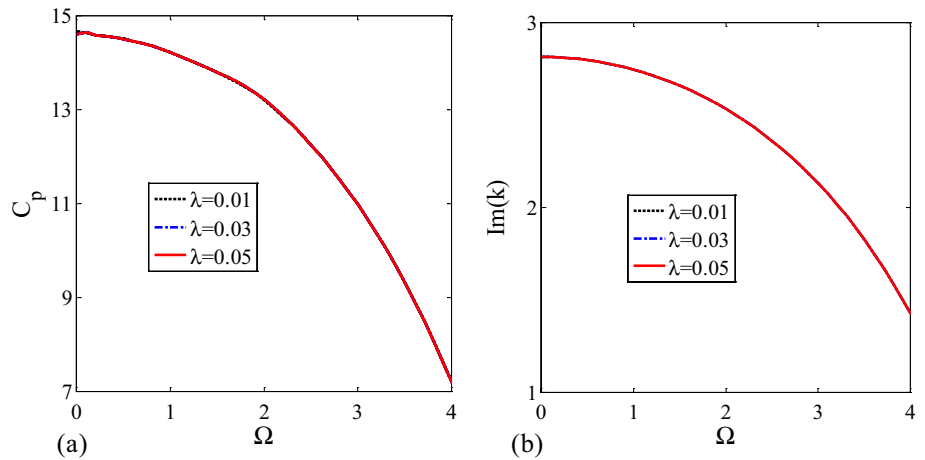


Table 3 Escape frequencies for the first five modes, $M=1$

	1st mode	2nd mode	3rd mode	4th mode	5th mode
$\lambda=0.02$	12.2	12.74	15.19	16.10	17.00
$\lambda=0.03$	8.13	8.97	10.12	10.73	11.90
$\lambda=0.04$	6.10	6.37	7.59	8.05	8.50
$\lambda=0.05$	4.88	5.38	6.07	6.44	7.14

structures without considering the temperature. Firstly, the results for an FGM cylindrical plate with a large radius thickness ratio ζ ($\zeta = 100$) are obtained from the SLPA ($N = 20$) and are shown with the results for an infinite FGM plate from the power series technique in Fig. 2. The material properties can be found in Ref. [29]. In Ref. [29], the phase velocity dispersion curves for pure ceramics, pure Cr and FGM composed of ceramics and Cr are given. For this comparison, only the case of FGM is given. It is evident that our results agree well with the open results,

which indicates that the SLPA is valid for the FGM cylindrical plates.

Then a comparison for the nonlocal nanostructures is given. The results from a uniform cylindrical plate with $\zeta = 100$, and those from a nonlocal graphene plate in Ref [44], are exhibited in Fig. 3. The phase velocity is

$$C_p = \frac{\omega}{\text{Re}(k)} = \frac{2\pi f}{\text{Re}(k)} \tag{20}$$

Obviously, the results by using the SLPA are consistent with the available ones [44], which are proved in Fig. 3. This comparison demonstrates that the SLPA is available for the nonlocal cylindrical plates.

3.2 Convergence of the SLPA

In this section, the convergence of the SLPA is discussed in Table 1. The material constants are listed in Table 2

Fig. 8 Phase velocity and attenuation curves of the first two Lamb-like waves, $\lambda=0.03$. **a** Phase velocity curves and **b** attenuation curves

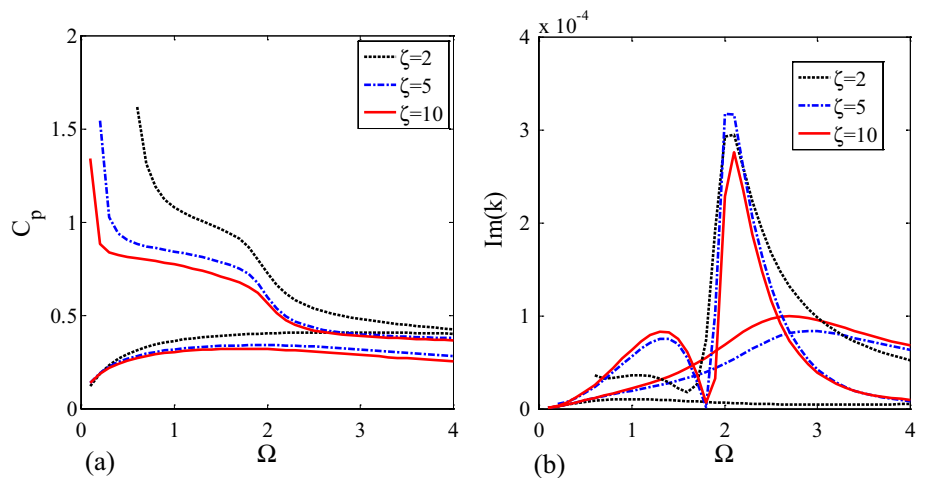


Fig. 9 Nonlocal effect on phase velocity with different ζ , $\lambda=0.03$. **a** 1st mode; **b** 2nd mode

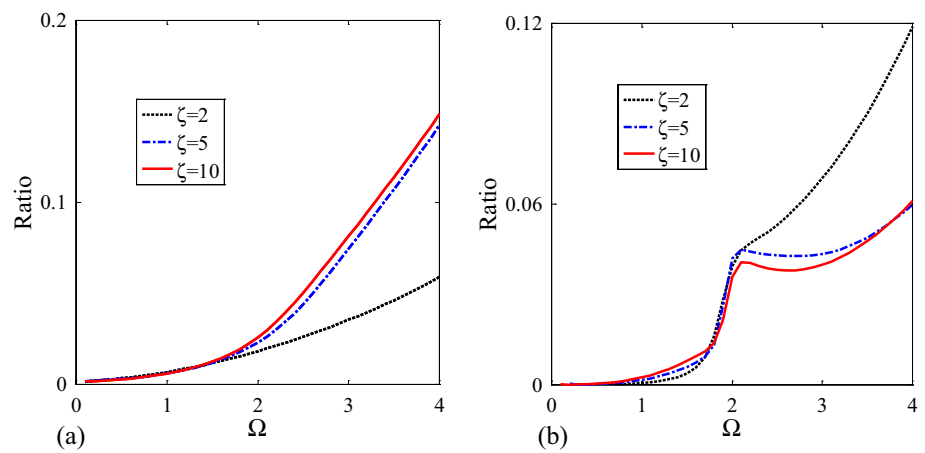
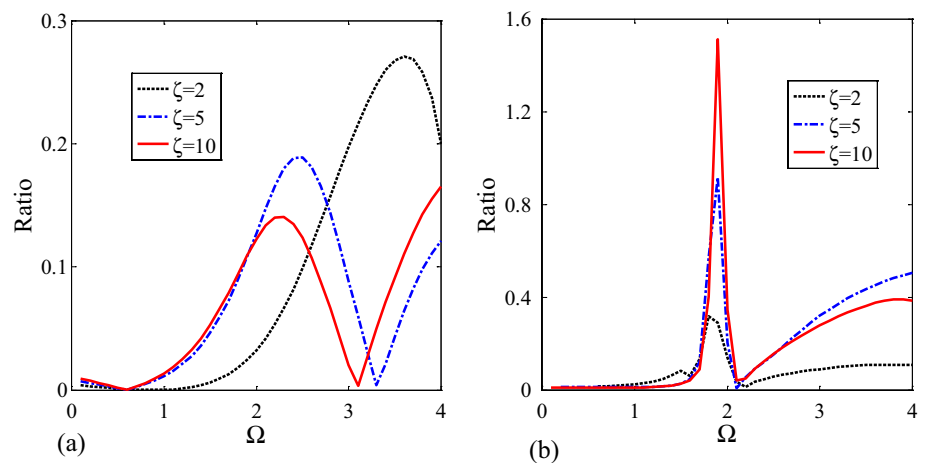


Fig. 10 Nonlocal effect on attenuation with different ζ , $\lambda=0.03$. **a** 1st mode; **b** 2nd mode



[45, 46]. The thermoelastic coupling constant $\eta=0.00249$. $M=1$, $\Omega=2$ and $\lambda=0.03$. The outer radius $b=5$, and the radius thickness ratio $\zeta=5$. For the first three Lamb-like wave modes, the real parts of the wavenumbers are convergent when $N=8$, and the imaginary ones are convergent when $N=10$. This indicates that the wavenumbers are convergent order by order, but their real parts converge faster than imaginary parts. For thermal wave mode, the real and imaginary parts of the wavenumbers are convergent when $N=4$. This example implies that the SLPA is convergent for both Lamb-like and thermal waves, but has different convergence rates. The convergence of thermal waves is much faster than that of Lamb-like waves.

3.3 Scale effect on phase velocity and attenuation

Figures 4, 5 give the phase velocity and attenuation curves of the first two Lamb-like waves with $\lambda=0.01, 0.03, 0.05$. At low frequencies, the nonlocal effect is weak on both dispersion and attenuation. But at high frequencies, the phase velocities decrease clearly with the increase in the nonlocal

parameter λ . From Fig. 5, the nonlocal effect is remarkable on attenuation. A bigger nonlocal parameter λ moves the peak value of attenuation to a lower frequency. The attenuations are enhanced by the nonlocal effect before the peak value and are suppressed after the peak value. It is noted that the attenuation of 1st mode with $\lambda=0.05$ (red line, Fig. 5a) in the red box is discordant. The reason is that the attenuation is oscillation near the escape frequencies, which is shown in Fig. 6.

Figure 7 exhibits the phase velocity and attenuation curves of the thermal waves and implies that their phase velocities and attenuations are almost not affected by λ . The reason can be found in the governing equation. λ is only in Eq. (5a–c), not in the heat conduction coupling Eq. (5d). Due to the small thermoelastic coupling constant ($\eta=0.00249$), the variation of thermal wave mode with different λ should be tiny.

It is noted that the waves in nanostructures only propagate between their cutoff frequencies and escape frequencies [27]. At the escape frequency, the phase velocity is zero. And above the escape frequency, the wave

phenomenon does not occur. As a crucial wave characteristic in nanostructures, the escape frequencies attract many attentions [27, 28, 32, 47]. Table 3 shows the escape frequencies of the first 5 modes in the FGM thermoelastic nanocylindrical plates. From Table 3, it is clearly seen that the escape frequencies are almost inversely proportional to λ . The reason can be found in the government equation. At the escape frequency, the phase velocity should be zero, and escape frequency ω_e should be finite. Thus, the wavenumber k trends to infinity. Considering Eq. (11), both sides of Eq. (10) are divided by k^2 ,

$$\omega_e^2 \frac{\rho}{\rho} \lambda^2 U - \frac{C_{11}}{C_{11}} U = 0 \quad (21a)$$

$$\omega_e^2 \frac{\rho}{\rho} \lambda^2 V - \frac{C_{55}}{C_{11}} V = 0 \quad (21b)$$

$$\omega_e^2 \frac{\rho}{\rho} \lambda^2 W - \frac{C_{13}}{C_{11}} U = 0 \quad (21c)$$

$$i\omega_e \frac{K_1}{K_1} \frac{\rho}{\rho} X + \eta \frac{\beta_1}{\beta_1} U = 0 \quad (21d)$$

Obviously, Eq. (21d) implies that there is no escape frequencies in thermal waves. Meanwhile, Eq. (21c) also does not yield the escape frequencies. Therefore, the escape frequencies only can be solved by Eqs. (21a, 21b) and are not affected by the temperature. More meaningful, the escape frequencies are inversely proportional to λ , but are unrelated to the geometrical radius and boundary conditions.

3.4 Outer radius thickness ratio

Although the radius thickness ratio ζ is unrelated to the escape frequency, it affects the phase velocity and attenuation significantly. The linear FGM nanocylindrical plates with $\zeta=2, 5, 10$ are considered here. $\lambda=0.03$. Figure 8 shows the phase velocity and attenuation curves of the first two Lamb-like modes with different ζ . It is obvious that the phase velocities increase with decreasing ζ for the two Lamb-like modes in Fig. 8a, which is similar to the case in classical theory. In addition, a larger ζ indicates a more considerable attenuation before the minimal attenuation.

The nonlocal effect on phase velocity and attenuation with different ζ is further analyzed in Figs. 9 and 10. The ratio is calculated as

$$\text{Ratio} = \left| \frac{\varphi^{\text{classical}} - \varphi^{\text{nonlocal}}}{\varphi^{\text{classical}}} \right| \quad (22)$$

ϕ is the C_p or $\text{im}(k)$ in Figs. 9 and 10, respectively. Before $\Omega=2$, Fig. 9 indicates that the strength of the nonlocal effects is close for different radius thickness ratios. However, after $\Omega=2$, the strength is different clearly. Specifically, a larger ζ means a more substantial nonlocal effect for the 1st mode, but implies a weaker nonlocal effect for the 2nd mode. For the attenuations in Fig. 10, the nonlocal effect is also close at low frequencies. Simultaneously, the max nonlocal effect moves to a lower frequency with a larger ζ . Besides, the nonlocal effect is weaker before its maximal value with a larger ζ , but is stronger after the max nonlocal effect. From Figs. 9 and 10, the nonlocal effect on attenuations is stronger than that on phase velocities at high frequencies.

4 Conclusions

In this article, a low cost and efficient SLPA is proposed to investigate the nonlocal effect on dispersion characteristics of the thermoelastic circumferential Lamb waves in inhomogeneous nanocylindrical plates. The nonlocal boundary condition can be imposed directly on the stress variables. More importantly, the original problem is translated into a generalized linear eigenvalue problem, which reduces the difficulty of solution. The study is meaningful for quality inspection and material property measurement of nanocylindrical plates. In general, we have the following discoveries:

A mathematical model is established for the thermoelastic circumferential Lamb waves in FGM nonlocal nanohollow cylinders on account of the nonlocal theory and is solved by the proposed SLPA.

Nonlocal effect is strong on both phase velocity and attenuation of Lamb-like waves, but is feeble on both phase velocity and attenuation of thermal waves.

The nonlocal effect enhances the attenuation of Lamb-like wave before the maximal attenuation and then suppresses it. The escape frequency is independent of the geometric radius, boundary conditions and temperature. It is just inversely proportional to nonlocal parameter.

Appendix

Defining

$$\begin{cases} u[n, m, L, s, j] = \int_a^b r^s \left(\frac{2r - b - a}{b - a} \right)^L Q_n(r) \frac{d^j}{dr^j} [(r - a)(r - b)Q_m(r)] dr \\ v[n, m, L, s, j] = \int_a^b r^s \left(\frac{2r - b - a}{b - a} \right)^L Q_n(r) \frac{d^j}{dr^j} Q_m(r) dr \end{cases}$$

The detailed of Eq. (10) are given here. The sum is applied when the symbols (j, p, l, s) occur more than once.

$$\begin{aligned} A_{11}^{n,m} &= \left(b^2 \lambda^2 \omega^2 \rho^{(j)} \rho^{(p)} - b^2 \rho^{(j)} C_{11}^{(p)} \right) \\ &v[n, m, j + p, 0, 0] B_{12}^{n,m} = ib \rho^{(j)} C_{11}^{(p)} \\ &(u[n, m, j + p, 1, 1] + 3u[n, m, j + p, 0, 0]) \\ &+ ib \rho^{(j)} C_{13}^{(p)} (-u[n, m, j + p, 0, 0] \\ &+ u[n, m, j + p, 1, 1]) - \frac{2j}{b - a} ib \rho^{(j)} C_{13}^{(p)} \\ &u[n, m, j + p - 1, 1, 0] C_{11}^{n,m} = \omega^2 \rho^{(j)} \rho^{(p)} \\ &(v[n, m, j + p, 2, 0] - \lambda^2 v[n, m, j + p, 1, 1] \\ &- \lambda^2 v[n, m, j + p, 2, 2]) + (-\rho^{(j)} C_{11}^{(p)} + \rho^{(j)} C_{13}^{(p)}) \\ &v[n, m, j + p, 0, 0] - \rho^{(j)} C_{13}^{(p)} v[n, m, j + p, 1, 1] \\ &+ \frac{2j}{b - a} \rho^{(j)} C_{13}^{(p)} v[n, m, j + p - 1, 1, 0] \end{aligned}$$

$$\begin{aligned} C_{13}^{n,m} &= \rho^{(j)} C_{11}^{(p)} (u[n, m, j + p, 1, 1] \\ &+ u[n, m, j + p, 0, 0]) \\ &+ \rho^{(j)} C_{13}^{(p)} (u[n, m, j + p, 2, 2] \\ &- u[n, m, j + p, 0, 0] + u[n, m, j + p, 1, 1]) \\ &- \frac{2j}{b - a} \rho^{(j)} C_{13}^{(p)} (u[n, m, j + p - 1, 2, 1] \\ &+ u[n, m, j + p - 1, 1, 0]) \end{aligned}$$

$$C_{14}^{n,m} = \omega^2 \rho^{(j)} \rho^{(p)} \beta_1^{(l)} u[n, m, j + p + l, 2, 0]$$

$$A_{22}^{n,m} = \left(\lambda^2 b^2 \omega^2 \rho^{(j)} \rho^{(p)} - b^2 \rho^{(j)} C_{55}^{(p)} \right) u[n, m, j + p, 0, 0]$$

$$\begin{aligned} B_{21}^{n,m} &= -3ib \rho^{(j)} C_{55}^{(p)} v[n, m, j + p, 0, 0] \\ &+ ib \rho^{(j)} C_{55}^{(p)} v[n, m, j + p, 1, 1] \\ &- \frac{2j}{b - a} ib \rho^{(j)} C_{55}^{(p)} v[n, m, j + p, 1, 0] \end{aligned}$$

$$B_{23}^{n,m} = ib \rho^{(j)} C_{55}^{(p)} (u[n, m, j + p, 1, 1] + u[n, m, j + p, 0, 0])$$

$$\begin{aligned} C_{22}^{n,m} &= \omega^2 \rho^{(j)} \rho^{(p)} (u[n, m, j + p, 2, 0] \\ &- \lambda^2 u[n, m, j + p, 1, 1] - \lambda^2 u[n, m, j + p, 2, 2]) \\ &+ \rho^{(j)} C_{55}^{(p)} (u[n, m, j + p, 2, 2] \\ &- 4u[n, m, j + p, 0, 0] + u[n, m, j + p, 1, 1]) \\ &- \frac{2j}{b - a} \rho^{(j)} C_{55}^{(p)} (u[n, m, j + p - 1, 2, 1] \\ &+ 2u[n, m, j + p - 1, 1, 0]) \end{aligned}$$

$$A_{31}^{n,m} = -b^2 \rho^{(j)} C_{13}^{(p)} v[n, m, j + p, 0, 0]$$

$$A_{33}^{n,m} = b^2 \lambda^2 \omega^2 \rho^{(j)} \rho^{(p)} u[n, m, j + p, 0, 0]$$

$$\begin{aligned} B_{12}^{n,m} &= ib \rho^{(j)} C_{13}^{(p)} (u[n, m, j + p, 1, 1] + 3u[n, m, j + p, 0, 0]) \\ &+ ib \rho^{(j)} C_{33}^{(p)} (-u[n, m, j + p, 0, 0] + u[n, m, j + p, 1, 1]) \\ &- \frac{2j}{b - a} ib \rho^{(j)} C_{33}^{(p)} u[n, m, j + p - 1, 1, 0] \end{aligned}$$

$$\begin{aligned} C_{31}^{n,m} &= \left(-\rho^{(j)} C_{13}^{(p)} + \rho^{(j)} C_{33}^{(p)} \right) v[n, m, j + p, 0, 0] \\ &- \rho^{(j)} C_{33}^{(p)} v[n, m, j + p, 1, 1] \\ &+ \frac{2j}{b - a} \rho^{(j)} C_{33}^{(p)} v[n, m, j + p - 1, 1, 0] \end{aligned}$$

$$\begin{aligned}
C_{33}^{n,m} &= \rho^{(j)} C_{13}^{(p)} (u[n, m, j + p, 1, 1] \\
&+ u[n, m, j + p, 0, 0]) \\
&+ \rho^{(j)} C_{33}^{(p)} (u[n, m, j + p, 2, 2] \\
&- u[n, m, j + p, 0, 0] + u[n, m, j + p, 1, 1]) \\
&- \frac{2j}{b-a} \rho^{(j)} C_{33}^{(p)} (u[n, m, j + p - 1, 2, 1] \\
&+ u[n, m, j + p - 1, 1, 0]) \\
&+ \omega^2 \rho^{(j)} \rho^{(p)} (v[n, m, j + p, 2, 0] \\
&- \lambda^2 v[n, m, j + p, 1, 1] - \lambda^2 v[n, m, j + p, 2, 2])
\end{aligned}$$

$$C_{34}^{n,m} = \omega^2 \rho^{(j)} \rho^{(p)} \beta_3^{(l)} u[n, m, j + p + l, 2, 0]$$

$$A_{41}^{n,m} = b^2 \eta (1 - i\omega\tau_0) \rho^{(j)} \beta_1^{(p)} v[n, m, j + p, 0, 0]$$

$$A_{44}^{n,m} = -i\omega b^2 \rho^{(j)} \rho^{(p)} K_1^{(l)} u[n, m, j + p + l, 0, 0]$$

$$\begin{aligned}
B_{42}^{n,m} &= ib\eta (1 - i\omega\tau_0) \rho^{(j)} \beta_1^{(p)} (u[n, m, j + p, 1, 1] + 3u[n, m, j + p, 0, 0]) \\
&+ ib\eta (1 - i\omega\tau_0) \rho^{(j)} \beta_3^{(p)} (u[n, m, j + p, 1, 1] - u[n, m, j + p, 0, 0]) \\
&- \frac{2j}{b-a} ib\eta (1 - i\omega\tau_0) \rho^{(j)} \beta_3^{(p)} u[n, m, j + p - 1, 1, 0]
\end{aligned}$$

$$\begin{aligned}
C_{41}^{n,m} &= -\eta (1 - i\omega\tau_0) \rho^{(j)} \beta_1^{(p)} v[n, m, j + p, 0, 0] \\
&+ \eta (1 - i\omega\tau_0) \rho^{(j)} \beta_3^{(p)} (v[n, m, j + p, 0, 0] - v[n, m, j + p, 1, 1]) \\
&- \frac{2j}{b-a} \eta (1 - i\omega\tau_0) \rho^{(j)} \beta_3^{(p)} v[n, m, j + p - 1, 1, 0]
\end{aligned}$$

$$\begin{aligned}
C_{43}^{n,m} &= \eta (1 - i\omega\tau_0) \rho^{(j)} \beta_1^{(p)} (u[n, m, j + p, 1, 1] \\
&+ u[n, m, j + p, 0, 0]) + \eta (1 - i\omega\tau_0) \\
&\rho^{(j)} \beta_3^{(p)} (u[n, m, j + p, 2, 2] - u[n, m, j + p, 0, 0]) \\
&+ u[n, m, j + p, 1, 1]) - \frac{2j}{b-a} \eta (1 - i\omega\tau_0) \rho^{(j)} \beta_3^{(p)} \\
&(u[n, m, j + p - 1, 2, 1] + u[n, m, j + p - 1, 1, 0]) C_{44}^{n,m} \\
&= i\omega \rho^{(j)} \rho^{(p)} K_3^{(l)} u[n, m, j + p + l, 2, 2] + i\omega \rho^{(j)} \rho^{(p)} K_1^{(l)} \\
&u[n, m, j + p + l, 1, 1] - (1 - i\omega\tau_0) \omega^2 \rho^{(j)} \rho^{(p)} \rho^{(s)} C_e^{(l)} \\
&u[n, m, j + p + s + l, 2, 0]
\end{aligned}$$

Acknowledgements This work was supported by National Natural Science Foundation of China under Grant No. 51975189, the Project funded by China Postdoctoral Science Foundation under Grant No. 2021M701102, the Henan University Science and Technology Innovation Team Support Plan under Grant No. 23IRTSTHN016 and the Innovative Research Team of Henan Polytechnic University under Grant No. T2022-4.

Declarations

Competing interest The authors declare that they have no known competing financial interests or personal relationships that could have appeared to influence the work reported in this paper.

References

- Hosseini-Ara R (2018) Nano-scale effects on nonlocal boundary conditions for exact buckling analysis of nano-beams with different end conditions. *J Braz Soc Mech Sci Eng* 40:144
- Zhao X, Zhu WD, Li YH (2020) Analytical solutions of nonlocal coupled thermoelastic forced vibrations of micro-/nano-beams by means of Green's functions. *J Sound Vib* 481:115407
- Hosseini SM (2017) Analytical solution for nonlocal coupled thermoelasticity analysis in a heat-affected MEMS/NEMS beam resonator based on Green–Naghdi theory. *Appl Math Model* 57:21–36
- He DZ, Shi DY, Wang QS et al (2021) Free vibration characteristics and wave propagation analysis in nonlocal functionally graded cylindrical nanoshell using wave-based method. *J Braz Soc Mech Sci Eng* 43:292
- Arash B, Wang Q, Liew KM (2012) Wave propagation in graphene sheets with nonlocal elastic theory via finite element formulation. *Comput Methods Appl Mech Eng* 223–224(3):1–9
- Sidhardh S, Ray MC (2019) Dispersion curves for Rayleigh–Lamb waves in a micro-plate considering strain gradient elasticity. *Wave Motion* 86:91–109
- Wu WB, Zhang HB, Jia F et al (2020) Surface effects on frequency dispersion characteristics of Lamb waves in a nanoplate. *Thin Solid Films* 697:137831
- Ebrahimi F, Seyfi A (2022) Wave propagation response of agglomerated multi-scale hybrid nanocomposite plates. *Waves Random Complex Med* 32(3):1338–1362
- Li CL, Han Q (2020) Analyzing wave propagation in graphene-reinforced nanocomposite annular plates by the semi-analytical formulation. *Mech Adv Mater Struct*. <https://doi.org/10.1080/15376494.2020.1736698>
- Aydogdu M (2014) Longitudinal wave propagation in multiwalled carbon nanotubes. *Compos Struct* 107:578–584
- Li CY, Chou TW (2006) Elastic wave velocities in single-walled carbon nanotubes. *Phys Rev B* 73(24):245407
- Zhang H, Yin X (2007) Guided circumferential waves in double-walled carbon nanotubes. *Acta Mech Solida Sin* 20(2):110–116
- Othman MIA, Mondal S (2019) Memory-dependent derivative effect on wave propagation of micropolar thermoelastic medium under pulsed laser heating with three theories. *Int J Numer Meths under Heat Fluid Flow* 30(3):1025–1046
- Ebrahimi F, Nouraei M, Seyfi A (2022) Wave dispersion characteristics of thermally excited graphene oxide powder-reinforced nanocomposite plates. *Waves Random Complex Med* 32(1):204–232
- Hosseini SM, Zhang CZ (2018) Coupled thermoelastic analysis of an FG multilayer graphene platelets-reinforced nanocomposite cylinder using meshless GFD method: a modified micromechanical model. *Eng Anal Boundary Elem* 88:80–92
- Dai JY, Liu YS, Tong GJ (2020) Wave propagation analysis of thermoelastic functionally graded nanotube conveying nanoflow. *J Vib Control*. <https://doi.org/10.1177/1077546320977044>
- Selim MM (2020) Propagation of longitudinal waves in a single-walled carbon nanotube under thermoelastic damping. *Micro Nano Lett*. 15(11):717–722
- Yang B, Droz C, Zine A et al (2020) Dynamic analysis of second strain gradient elasticity through a wave finite element approach. *Compos Struct* 263:113425
- Eringen AC (1983) On differential equations of nonlocal elasticity and solutions of screw dislocation and surface waves. *J Appl Phys* 54(9):4703–4710
- Gu BD, He TH (2021) Investigation of thermoelastic wave propagation in Euler–Bernoulli beam via nonlocal strain gradient

- elasticity and G–N theory. *J Vib Eng Technol.* <https://doi.org/10.1007/s42417-020-00277-4>
21. Ma LH, Ke LL, Wang YZ et al (2018) Wave propagation analysis of piezoelectric nanoplates based on the nonlocal theory. *Int J Struct Stab Dyn* 18(4):1850060
 22. Hosseini SM, Sladek J, Sladek V (2020) Nonlocal coupled photo-thermoelasticity analysis in a semiconducting micro/nano beam resonator subjected to plasma shock loading: a Green–Naghdi-based analytical solution. *Appl Math Model* 88(4):631–651
 23. Hosseini SM, Zhang CZ (2019) Nonlocal coupled thermoelastic wave propagation band structures of nano-scale phononic crystal beams based on GN theory with energy dissipation: an analytical solution. *Wave Motion* 92:102429
 24. Patra S, Ahmed H, Saadatzi M et al (2019) Experimental verification and validation of nonlocal peridynamic approach for simulating guided Lamb wave propagation and damage interaction. *Struct Health Monit* 18(5–6):1789–1802
 25. Eltahir MA, Omar FA, Abdalla WS et al (2019) Bending and vibrational behaviors of piezoelectric nonlocal nanobeam including surface elasticity. *Waves Random Complex Med* 29(2):264–280
 26. Yan DJ, Chen AL, Wang YS et al (2017) Propagation of guided elastic waves in nanoscale layered periodic piezoelectric composites. *Eur J Mech A Solids* 66:158–167
 27. Zhang LL, Liu JX, Fang XQ et al (2014) Effects of surface piezoelectricity and nonlocal scale on wave propagation in piezoelectric nanoplates. *Eur J Mech A Solids* 46(4):22–29
 28. Park J, Kausel E (2004) Numerical dispersion in the thin-layer method. *Comput Struct* 82(7/8):607–625
 29. Cao XS, Feng J, Jeon I (2011) Calculation of propagation properties of Lamb waves in a functionally graded material (FGM) plate by power series technique. *NDT E Int* 44(1):84–92
 30. Gravenkamp H, Birk C, Song C (2015) Simulation of elastic guided waves interacting with defects in arbitrarily long structures using the scaled boundary finite element method. *J Comput Phys* 295:438–455
 31. Chaki MS, Singh AK (2020) Anti-plane wave in a piezoelectric viscoelastic composite medium: a semi-analytical finite element approach using PML. *Int J Appl Mech* 12(2):2050020
 32. Chen JY, Guo JH, Pan EN (2017) Wave propagation in magneto-electro-elastic multilayered plates with nonlocal effect. *J Sound Vib* 400:550–563
 33. Elmaimouni L, Lefebvre JE, Zhang V et al (2007) A polynomial approach to the analysis of guided waves in anisotropic cylinders of infinite length. *Wave Motion* 42(2):177–189
 34. Hosseini SM, Zhang CZ (2021) Band structure analysis of Green–Naghdi-based thermoelastic wave propagation in cylindrical phononic crystals with energy dissipation using a meshless collocation method. *Int J Mech Sci* 209:106711
 35. Zheng MF, He CF, Lu Y et al (2018) State-vector formalism and the Legendre polynomial solution for modelling guided waves in anisotropic plates. *J Sound Vib* 412:372–388
 36. Li Z, Yu JG, Zhang XM et al (2020) Guided wave propagation in functionally graded fractional viscoelastic plates: a quadrature free Legendre polynomial method. *Mech Adv Mater Struct.* <https://doi.org/10.1080/15376494.2020.1860273>
 37. Othmani C, Zhang H (2020) Lamb wave propagation in anisotropic multilayered piezoelectric laminates made of PVDF- θ° with initial stresses. *Compos Struct* 240:112085
 38. Yu JG, Wang XH, Zhang XM et al (2022) An analytical integration Legendre polynomial series approach for Lamb waves in fractional order thermoelastic multilayered plates. *Math Methods Appl Sci* 45(12):7631–7651
 39. Liu CC, Yu JG, Zhang XM et al (2020) Reflection behavior of elastic waves in the functionally graded piezoelectric microstructures. *Eur J Mech A Solids* 81:103955
 40. Liu CC, Yu JG, Zhang B et al (2021) Analysis of Lamb wave propagation in a functionally graded piezoelectric small-scale plate based on the modified couple stress theory. *Compos Struct* 265(2):113733
 41. Bagri A, Eslami MR (2004) Generalized coupled thermoelasticity of disks based on the Lord–Shulman model. *J Therm Stresses* 27(8):691–704
 42. Bachher M, Sarkar N (2019) Nonlocal theory of thermoelastic materials with voids and fractional derivative heat transfer. *Waves Random Complex Med* 29(4):595–613
 43. Arash B, Ansari R (2010) Evaluation of nonlocal parameter in the vibrations of single-walled carbon nanotubes with initial strain. *Phys E Low Dimens Syst Nanostruct* 42(8):2058–2064
 44. Liu H, Yang TL (2012) Elastic wave propagation in a single-layered graphene sheet on two-parameter elastic foundation via nonlocal elasticity. *Phys E* 44:1236–1240
 45. Al-Qahtani H, Datta SK (2004) Thermoelastic waves in an anisotropic infinite plate. *J Appl Phys* 96(7):3645–3658
 46. Li JF (2012) Thermal structure coupled computer simulation of multilayer protection/insulation system. Master's thesis of Harbin University of Technology (in Chinese)
 47. Chakraborty A (2007) Wave propagation in anisotropic media with nonlocal elasticity. *Int J Solids Struct* 44(17):5723–5741

Publisher's Note Springer Nature remains neutral with regard to jurisdictional claims in published maps and institutional affiliations.

Springer Nature or its licensor (e.g. a society or other partner) holds exclusive rights to this article under a publishing agreement with the author(s) or other rightsholder(s); author self-archiving of the accepted manuscript version of this article is solely governed by the terms of such publishing agreement and applicable law.